

# Chandra Analysis of Abell 496 - No Chemical Gradients Across Cold Fronts

Renato Dupke

University of Michigan, Ann Arbor

Raymond E. White III

University of Alabama, Tuscaloosa

Received \_\_\_\_\_; accepted \_\_\_\_\_

## ABSTRACT

We present the results of a spatially-resolved spectroscopic analysis of the galaxy cluster Abell 496 with the S3 chip on-board the *Chandra* satellite. We confirm the presence of a central positive temperature gradient consistent with a cooling flow, but with a minimum gas temperature of  $\sim 0.5\text{--}0.9$  keV. The cluster also exhibits sharp edges in gas density and temperature which are consistent with “cold front” substructures. The iron abundance profile is not radially symmetric relative to the cluster center. Towards the direction of the most prominent (northerly) cold front, the iron abundance is roughly flat, with nearly solar values. In the opposite (southerly) direction from the center, the iron abundance distribution shows an “off-center” peak. Various abundance ratios suggest that the heavy elements in the central regions of the cluster are dominated by SN Ia ejecta. However, for radii greater than  $100 h_{50}^{-1}$  kpc, the abundance ratios vary in such a way that different abundance ratios provide very different estimates of the proportion of SN Ia/II ejecta. Nonetheless, observed abundances and abundance ratios are continuous across the cold fronts, which suggests that the cold fronts are not likely to be the result of a subcluster merger. We suggest instead that the cold fronts in A496 are caused by “sloshing” of the central cooling flow gas, induced by the motion of the cD about the cluster center.

*Subject headings:* cooling flows — galaxies: clusters: individual (Abell 496) — intergalactic medium — X-rays: galaxies: clusters

## 1. Introduction

*Chandra* satellite observations have revealed a wealth of X-ray structures in the cores of galaxy clusters, including X-ray plumes (e.g. Sanders & Fabian 2002), cavities (e.g. McNamara et al. 2000), and “cold fronts” (e.g. Markevitch et al. 2000; Vikhlinin et al. 2001; Mazzotta et al. 2001). Cold fronts (hereafter CF) are sharp surface brightness discontinuities (widths are typically smaller than the electron mean free path) characterized by a jump in gas temperature, accompanied by a fall in X-ray surface brightness such that the gas pressure remains continuous across the front. Thus, these structures differ from bow shocks (e.g. Markevitch et al. 2002) and are often attributed to subsonic (transonic) motions of accreted substructures (Markevitch et al. 2000, 2001; Vikhlinin et al. 2001)

The incidence of gaseous substructures at the centers of clusters suggests that cluster cores are very dynamic, even when there are no obvious signs of merging (such as in cooling flow clusters with regular isophotes). In this *Letter* we show that this is the case for A496. This cluster is a typical, bright, nearby ( $z \approx 0.032$ ), apparently well-behaved cooling flow cluster. In a joint *Ginga* and *Einstein* analysis of A496, White et al. (1994) found evidence for a central metal abundance enhancement. This was corroborated by *ASCA* (e.g. Dupke & White 2000a), *SAX* (Irwin & Bregman 2001) and *XMM* (Tamura et al. 2001) with greater statistical significance. Furthermore, Dupke & White (2000a) also discovered radial gradients in various abundance *ratios*, indicating that the gas in the central 2-3' has a higher proportion of SN Ia ejecta ( $\sim 70\%$ ) than the outer parts of the cluster.

Spectral analysis of radially averaged annuli with *XMM* is roughly consistent with *ASCA* results (Tamura et al. 2001). The spatial resolution achieved by the instruments on-board *XMM* are very limited in establishing fine correlations between spatial substructures, such as CFs, and spectral parameters such as metal abundances and temperatures. However, this analysis is important since it provides clues about the nature of such

structures. For example, if CFs are caused by the passage of a high velocity gas clump through the intracluster gas, the sharp surface discontinuity should be accompanied by chemical discontinuities as well, representing the enrichment history of the two different systems. This kind of analysis can be performed best with *Chandra*, given its high angular resolution. In this *Letter* we describe the discovery of CFs in A496 and search for chemical discontinuities across them. A more detailed analysis of the gas mass distribution will be published elsewhere. All distances shown are calculated assuming a  $H_0 = 50 \text{ km s}^{-1}\text{Mpc}^{-1}$  and  $\Omega_0 = 1$ . At the distance of this cluster  $1'' \approx 0.95 \text{ kpc}$ .

## 2. Data Reduction

A496 was observed by *Chandra* ACIS-S3 in July 2000 and October 2001, for 20 and 10 ksec, respectively. In both cases the cluster was centered on the S3 chip. The first observation was largely contaminated by flares, and will not be analyzed here. We used Ciao 2.2.1 with CALDB 2.9 to screen the data. Two short flare-like periods were extracted and the resulting exposure time is 8.7 ksec. A gain map correction was applied together with PHA and pixel randomization. The ACIS particle background was cleaned as prescribed for VFaint mode. Point sources were extracted and the background used in spectral fits was generated from blank-sky observations using the `acis_bkgrnd_lookup` script. Here we show the results of spectral fits with XSPEC V11.2 (Arnaud 1996) using the `mekal` and `vmekal` thermal emission models. An isobaric cooling flow model `cflow`, was used for the spectral fittings of the inner regions, where the minimum cooling flow temperature ( $kT_{\text{min}}^{\text{cf}}$ ) was allowed to vary. Metal abundances are measured relative to the solar photospheric values of Anders & Grevesse (1989). Galactic photoelectric absorption was incorporated using the `wabs` model (Morrison & McCammon 1983). Spectral channels were grouped ( $>25 \text{ cnt/chan}$ ). Energy ranges were restricted to 0.5–8.5 keV. Errors are  $1-\sigma$

unless stated otherwise.

In order to compensate for the recently detected degradation of ACIS low energy quantum efficiency (QE), we used the most recent `corrarf` routine, which applies the absorption model `acisabs` (Chartas & Getman (2002)) to the effective area file generated by the CIAO tool `mkarf`. The resulting spectral fits have significantly reduced column densities (compared to the prior, artificially inflated values), but they have a mild dependence on the low energy cut-off used in the data. Low-energy metal abundances are also affected by the low energy cut-off value. Since we are looking for *relative* changes of spectral parameters through different directions inside the cluster, this problem does not affect our conclusions. However, the absolute values of some abundances and of the hydrogen column density should not be considered definitive since the low energy calibration is still evolving.

### 3. Results

#### 3.1. Cold Front

Figs. 1a and b show the X-ray image of A496. One can clearly see the sharp edge in surface brightness (SB) towards the north. Fig. 1a shows the directions towards *sb\_sharp* and *sb\_smooth* used to extract SB profiles. We also extracted SB profiles for the perpendicular directions (labeled *sb\_east* and *sb\_west*) for comparison. Fig. 1b shows the extraction regions used for spectral analysis, which are separated in semi-annuli with opening angles close to  $180^\circ$  towards the *sharp* direction and towards the opposite direction (hereafter called *smooth*). The semi-annuli were chosen to maximize photon statistics at several radii along the direction of interest (perpendicular to the SB edge).

Fig. 2 shows a comparison between the SB and temperature profiles. The temperatures were typically obtained through spectral fits using an absorbed `mekal` model, where the

hydrogen column density was a free parameter. Despite the apparent smoothness of the average SB profile (in black) it is clear that the density profiles towards different directions are irregular, especially along the *sb\_sharp–sb\_smooth* axis. The position of the sharp edge is shown by a red vertical red line (at  $r \approx 82$  kpc), where there is a strong decline in SB: a factor of  $\sim 2$  within  $\sim 10$  kpc, accompanied by a temperature rise from  $4.06^{+0.26}_{-0.28}$  keV to  $5.20^{+0.46}_{-0.42}$  keV. The gas pressure is roughly constant (within the errors) throughout the discontinuity, which is consistent with the CF phenomenon (Markevitch et al. 2000). The temperature profile within 82 kpc also exhibit strong anisotropies. Towards the *sharp* direction the temperature rises more or less steadily from  $1.66^{+0.13}_{-0.11}$  to  $4.06^{+0.26}_{-0.28}$  keV. The addition of a cooling flow model in the inner  $10''$  does not change significantly the best-fit parameters and does not improve the  $\chi^2_{\nu}$ . The minimum cooling flow temperature found is  $kT_{\min}^{\text{cf}} \sim 0.96$  keV, with an associated mass deposition rate of  $\sim 5 M_{\odot} \text{ yr}^{-1}$ . Towards the *smooth* side the temperature rises steadily outward to a radial distance of 25 kpc and then rises steeply from  $2.73^{+0.25}_{-0.21}$  keV to  $4.30^{+0.48}_{-0.42}$  keV within a span of 15 kpc. The temperature profile suggests the presence of a secondary CF at  $\sim 25$  kpc, although there is no clear association with a SB drop within the same region. This may be due to the azimuthally symmetric binning geometry being a poor match to the oblique front structure to the south. At  $r \gtrsim 25$  kpc the gas temperature has a flat profile throughout. Spectral fittings of the central region on the *smooth* side are significantly improved with the addition of a cooling flow component. The resulting best fit temperature is  $3.2 \pm 0.7$  keV with a mass deposition rate of  $4.6 \pm 1.3 M_{\odot} \text{ yr}^{-1}$  and  $kT_{\min}^{\text{cf}} = 0.57^{+0.25}_{-0.49}$  keV.

### 3.2. Metal Abundance and Abundance Ratios Distribution

The spectral fittings when individual abundances were allowed to vary independently (*vmekal*) were slightly better than those where the abundances were tied to their solar

ratios, as previously found in *ASCA* data by Dupke & White (2000a). Fig. 3 shows temperature and abundance profiles of the best constrained elements (Fe, Si, O and S) in radial slices through the whole region analyzed in this work. Temperature and iron abundance ( $A_{\text{Fe}}$ ) anisotropies are clearly seen. The radial binning in Fig. 3 is larger than that in Fig. 2. This choice of binning increased the significance and magnitude of the temperature jump across the CF. The temperature jumps from  $3.57^{+0.23}_{-0.20}$  keV to  $5.60^{+0.51}_{-0.32}$  keV across the CF. Note that  $A_{\text{Fe}}$  does not change across the CF. The  $A_{\text{Fe}}$  profile is remarkably flat towards the *sharp* direction, with an average value of  $\sim 0.75$  solar. Towards the *smooth* direction  $A_{\text{Fe}}$  has a marginal rise from  $0.59^{+0.17}_{-0.10}$  solar at the center to  $0.87^{+0.17}_{-0.15}$  solar at  $\sim 70$  kpc. It then declines again to a minimum value of  $0.49^{+0.10}_{-0.08}$  solar towards the outer regions. We used the F-test to estimate the significance of the Fe abundance gradient towards the *smooth* side. We verified that the abundance gradient in the fourth and fifth radial bins is significant at  $\gtrsim 98\%$  confidence. This off-center abundance peak is similar to that found by Sanders & Fabian (2002) in A3526 and by Johnstone et al. (2002) in A2199. However, the addition of a cooling flow component to the innermost spatial bin ( $< 22''$ ) improves the spectral fits significantly, increasing the best fit  $A_{\text{Fe}}$  to  $1.52 \pm 0.45$  solar, eliminating the central depression. Adding the same cooling flow component to the *sharp* central region does not change significantly  $A_{\text{Fe}}$ .

The distribution of the silicon abundance ( $A_{\text{Si}}$ ) shows a negative gradient towards both *sharp* and *smooth* sides. The gradient is steeper but consistent with that measured in full ( $0-2\pi$ ) annular regions with *XMM* data (Tamura et al. 2001). The oxygen abundance ( $A_{\text{O}}$ ) tends to rise radially towards both *sharp* and *smooth* directions. By simultaneously fitting the spectra of the inner bins from the *sharp* and *smooth* sides, we measured a best fit central  $A_{\text{O}}$  of  $0.60^{+0.24}_{-0.36}$  solar, which is significantly lower than in the outermost bin of the *smooth* side ( $A_{\text{O}} = 1.61^{+0.6}_{-0.45}$  solar). This trend is consistent with *ASCA* SIS measurements (Dupke & White 2000a) but was not observed by Tamura et al. (2001). However, the sizes of the

extraction regions used in their work are not directly comparable to ours. Furthermore, as it can be seen from Fig. 3, their choice of region configuration can smooth out the  $A_O$  gradient due to the asymmetries in the abundance profile. The central absolute  $A_O$  values are higher than those found in a preliminary *Chandra* analysis of Dupke & White (2001), who used the least flare-contaminated period of a previous observation of A496 without any correction for QE degradation. The sulfur abundance is not well constrained and is consistent with being flat. Overall,  $A_{Si}$  and  $A_O$  distributions are consistent with radial gradients, but there are no discontinuities across the CFs.

In Fig. 4 we plot the abundance ratio profiles. Since different types of SNe have characteristic mass yields for different elements, their relative pollution rate can be measured, in principle, via abundance ratios (cf. Loewenstein & Mushotzky 1996), which in turn help us to determine the enrichment history of the gas. It can be seen that both O/Fe and Si/Fe are consistent with a central ( $r \lesssim 80$  kpc) dominance of SN Ia ejecta. However, both ratios show radial gradients and their outer values do not agree on a single proportion of SN Ia/II ejecta at a given exterior radius. The low Si/Fe ratios between 100–200 kpc are driven mainly by the low values of  $A_{Si}$  in that region. A positive gradient in the O/Fe was also detected in Dupke & White (2001) and it is unlikely that further calibration improvements will affect significantly the O/Fe profile, although the absolute values of the individual abundances are more uncertain. The poor photon statistics of our observation do not allow us to constrain other ratios well enough to check for the self-consistency of abundance ratios using different theoretical SN models, as in Dupke & White (2000b). However, independently of absolute normalizations, it is clear that there is no significant change in abundance ratio distribution across the sharp boundaries of the CFs.



#### 4. Discussion: The Nature of Cold Fronts

Two recently proposed hypotheses for generating CFs in clusters involve the infall of galaxy groups into the larger clusters. In some cases the substructures are sub(/trans)sonic remnants of mergers (e.g. Markevitch et al. 2000; Vikhlinin et al. 2001). In other cases, such as A1795 (Markevitch et al. 2001), it is proposed that the infall of a small gravitational substructure disturbs the central gravitational potential of the main cluster, causing low-entropy gas in the center to oscillate around some equilibrium position (the “sloshing” hypothesis). In both cases one expects the CF to be a surface discontinuity between a cold core moving through hotter, diffuse intracluster gas, with inefficient mixing between the different gas phases across the surface discontinuity. If this were true for A496 one should expect to see different metal enrichment histories across the CF. We find instead that abundances and abundance ratios are continuous across CFs, a result that is independent of calibration uncertainties in determining the absolute abundances of individual elements.

The data is roughly consistent with a model where the cD is oscillating around the clusters’ potential well. This model is similar to that suggested for A1795 (Fabian et al. 2001). In both clusters the CFs are aligned with the most likely projected axis of motion of the cD. This axis is inferred by analysis of the direction of the main extension of optical filaments (see Fabian et al. 1981), X-ray and optical isophotal elongation. The cDs in both systems have similar peculiar velocities after correcting for substructure (Bird 1994). In this model the cD would be dragging/smearing SN Ia Fe enriched cold gas within the spatial oscillation length ( $\sim 80$  kpc), which defines the distance to farthest CF observed. The most likely evolutionary time frame for this model would place the cD in A496 moving south beginning to generate a second CF. The motion of the cD may add to other competing core heating mechanisms, which may keep  $kT_{\min}^{\text{cf}} \sim 1$  keV. A detailed analysis of this model and other alternates is beyond the scope of this *Letter* and will be published elsewhere.

The investigation of the behavior of abundances and their ratios across SB discontinuities in the cores of other clusters will allow us to determine whether such structures are typically induced externally, via subcluster mergers, or internally, perhaps through sloshing associated with cD motion.

We are very grateful to P. Plucinsky, A. Prestwitch and H. Tananbaum for their help in obtaining a reobservation of A496. We acknowledge support from NASA through *Chandra* award number GO 0-1085X, issued by the *Chandra* X-ray Observatory Center, which is operated by the Smithsonian Astrophysical Observatory for and on behalf of NASA under contract NAS8-39073. RAD was also partially supported by NASA grant NAG 5-3247. RAD also thanks J. Irwin, J. Bregman and E. Lloyd-Davies for helpful discussions.

## REFERENCES

- Anders, E. & Grevesse N. 1989, *Geochimica et Cosmochimica Acta*, 53, 197
- Arnaud, K. A. 1996, in *Astronomical Data Analysis Software and Systems V*, ASP Conf. Series volume 101, eds. Jacoby, G. & Barnes, J., p.17
- Bird, C. 1994, *AJ*, 107, 1637
- Chartas, G. & Getman, K. 2002,  
[www.astro.psu.edu/users/chartas/xcontdir/xcont.html](http://www.astro.psu.edu/users/chartas/xcontdir/xcont.html)
- Dupke, R. A. & White, R. E. III 2000a, *ApJ*, 537, 123
- Dupke, R. A. & White, R. E. III 2000b, *ApJ*, 528, 139
- Dupke, R. A. & White, R. E. III 2001, in “The X-ray Universe at Sharp Focus,” eds. Schlegel, E. M. & Vrtilik, S. B., p. 377
- Fabian, A. C. et al. 1981, *MNRAS*196, 35
- Fabian, A. C. et al. 2001, *MNRAS*321, 33
- Irwin, J. & Bregman, J. 2001, *ApJ*, 546, 150
- Loewenstein, M. & Mushotzky, R. F. 1996, *ApJ*, 466, 695
- Markevitch M. et al. 2000, *ApJ*, 541, 542
- Markevitch, M., Vikhlinin, A., & Mazzotta, P. 2001, *ApJ*, 562, L153
- Markevitch, M. et al. 2002, *ApJ*, 567, 27
- Mazzotta, P. et al. 2001, *ApJ*, 555, 205
- McNamara, B. R. et al. 2000, *ApJ*, 534, 135
- Morrison, R. & McCammon, D. 1983, *ApJ*, 270, 119
- Mushotzky, R. F. et al. 1996, *ApJ*, 466, 686

Nomoto, K. et al. 1997a, Nuclear Physics A, Vol. A621, 467c

Nomoto, K. et al. 1997b, Nuclear Physics A, Vol. A616, 79

Sanders, J. S. & Fabian, A. C. 2002, MNRAS, 331, 273

Tamura, T. et al. 2001, A&A, 379, 107

Vikhlinin, A., Markevitch, M., & Murray, S. 2001, ApJ, 551, 160

White, R. E. III, Day, C. S. R., Hatsukade, I., & Hughes, J. P. 1994, ApJ, 433, 583

## Figure Captions

Fig. 1.— A496 Extraction Regions. X-ray exposure corrected image (in the range 0.3–10 keV). One pixel corresponds to  $4''$  and North is to the top. (a) The four different directions selected for image analysis. (b) Semi-annuli extraction regions used in the spectral analysis.

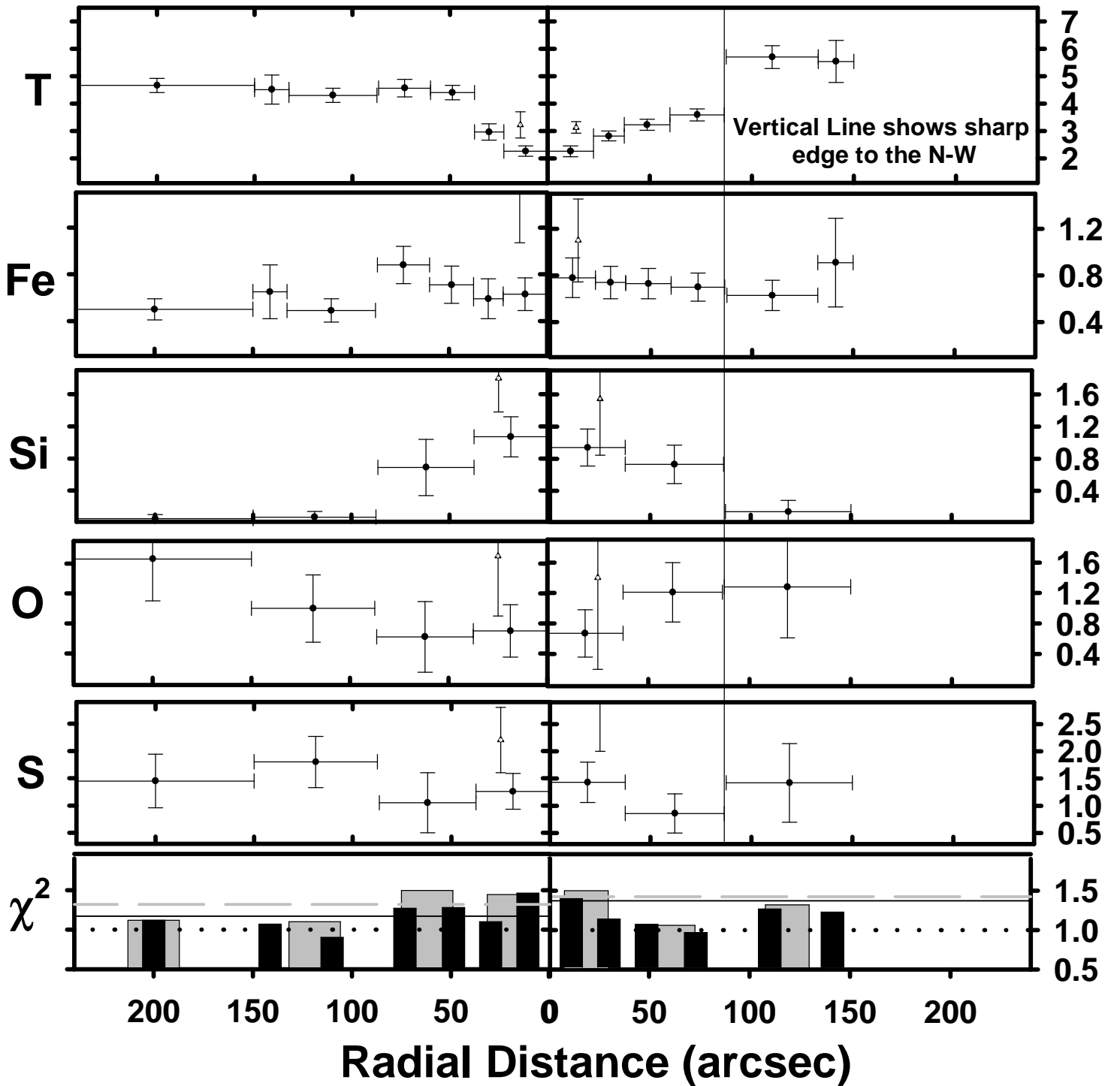
Fig. 2.— Temperature and Density Profiles. *Top*: Best-fit gas temperature distributions towards the *sharp* (red) and *smooth* (blue) directions obtained using a `wabs mekal` spectral model and also with the addition of a `cflow` component for the central bin (points with vertical error bars only). The extraction regions correspond to those shown in Fig. 1b. Errors are  $1-\sigma$  confidence. Vertical red line indicates the position of the sharp edge towards the *sharp* direction. *Middle*: Surface brightness profiles towards different directions indicated in Fig. 1a. Similar color notation is applied for the *sb\_sharp* and *sb\_smooth* directions. *East* and *west* directions are also shown in green and dark yellow colors, respectively. Splines connecting surface brightness values for all directions are also shown (with normalizations reduced by a factor of 2 for illustration purposes). We also show the overall (full annuli) surface brightness profile (black line with normalization reduced by a factor of 4). *Bottom*: Reduced chi-squared for the spectral fittings shown on *Top* plot, using the same color notation. Spectral fittings typically have 50–100 degrees of freedom. Horizontal lines show the values for the cases where a `cflow` spectral component is added in the spectral fits for the central bin.

Fig. 3.— Individual Metal Abundance & Temperature Distributions. Results from spectral fittings of regions along the line of symmetry of the sharp edge. The zero point represent the X-ray center. The vertical line indicates the position of the CF. Metal abundances are denoted by the element notation. The bin size used for Si, O and S is larger than that of T and Fe to improve statistics. Fittings with an additional `cflow` component to the `wabs Vmekal` are also shown for the central bin in all plots by points with vertical error bars only.

The reduced chi-squared for the spectral fittings are shown on the bottom plot for all bin sizes (black for T, Fe and gray for Si, O, S). Spectral fittings typically have 100–200 and 150–250 degrees of freedom for thin and thick bins, respectively. Horizontal lines show the values for the cases where a `cflow` component is added to the spectral models used to fit data from the central bin (black solid lines for T, Fe and gray dashed lines for Si, O, S).

Fig. 4.— Individual Metal Abundance Ratio Distributions. Notation is analogous to Fig. 3. Dotted and dashed horizontal lines show the predicted values for 100% SN Ia contamination and 100% SN II contamination, respectively, as described by Nomoto et al. 1997a,b. Central bin size is  $37.5''$ .

# Away from Sharp Edge Towards Sharp Edge



Away from Sharp Edge

Towards Sharp Edge

